PHOTONICS Research

Exploitation of geometric and propagation phases for spin-dependent rational-multiple complete phase modulation using dielectric metasurfaces

Ata Ur Rahman Khalid,[1,†] Fu Feng,[1,†] Naeem Ullah,[2] Xiaocong Yuan,[1,4] and Michael Geoffrey Somekh[1,3,5]

[1]Nanophotonics Research Center, Shenzhen Key Laboratory of Micro-Scale Optical Information Technology & Institute of Microscale Optoelectronics, Shenzhen University, Shenzhen 518060, China
[2]Beijing Engineering Research Center for Mixed Reality and Advanced Display, School of Optics and Photonics, Beijing Institute of Technology, Beijing 100081, China
[3]Faculty of Engineering, University of Nottingham, Nottingham NG7 2RD, UK
[4]e-mail: xcyuan@szu.edu.cn
[5]e-mail: mike.somekh@szu.edu.cn

Received 2 August 2021; revised 31 January 2022; accepted 1 February 2022; posted 2 February 2022 (Doc. ID 439094); published 11 March 2022

Metasurfaces have drawn considerable attention in manipulation of electromagnetic waves due to their exotic subwavelength footprints. Regardless of immense progress of polarization-dependent flat optics, the realization of on-device switchable complete phase multiplication is still missing from design multifunctional devices. Here, by combining geometric and propagation phases, a generalized design principle is proposed that can achieve switchable integer or fractional multiple complete phase modulation in transmitted circularly cross-polarized light by switching the handedness of incident polarization. As a proof of concept, two types of spin-dependent bifunctional wavefront manipulating devices, including switchable beam splitter/beam deflector and spin-to-orbital angular momentum converter designs are numerically realized. It is believed that the proposed single-cell spin-switchable rational-multiple complete-phase-modulation design principle based on combined propagation and geometric phases has great potential to underpin the development of meta-optics-based multifunctional operations in the field of integrated optics, imaging, and optical communication.

https://doi.org/10.1364/PRJ.439094

1. INTRODUCTION

Multifunctional planar on-chip photonic devices will play a fundamental role in several applications such as imaging, microscopy, and communication. In the past few years, subwavelength-sized engineered structures named metasurfaces have attracted tremendous research attention to manipulate electromagnetic (EM) waves and provide a platform to replace the traditional optical components [1,2]. By using these ultrathin elements, the amplitude, phase, and polarization of light in transmission/reflection can be precisely tailored for wavefront control such as metasurface holograms [3–10], vortex beam generators [11–13], flat lenses [14–19], and anomalous beam deflection [1,20] in linear and nonlinear regimes [21–25].

Metasurfaces can impart the desired phase profile on distinct input polarizations. In general, polarization-dependent phase can be classified into two categories. (1) The propagation (or structural/dynamic/retardation) phase, which mainly comes from the spatial structural parameters and material, contributes to attaching independent and arbitrary phase profiles on each of linearly orthogonal polarization. (2) The geometric phase follows the rotation-dependent Pancharatnam–Berry (PB) mechanism, which imposes the opposite (in sign) and equal phase to two circularly polarized (CP) channels. By combining both structural parameters and rotation, both propagation and geometric phases can be merged, which can result in any arbitrary phase profile on orthogonal CP polarization channels [26,27].

This hybrid phase-modulation scheme has been studied in many applications such as holography [26,28], switchable spiral contrast imaging [29], on-demand control of optical tweezers and spanning [30], orbital angular momentum (OAM) generation [31,32], and metalenses [33,34]. Owing to its design flexibility, this scheme is favorable in uncovering unexplored potentials in flat EM devices. For instance, one of the CP cross-polarized channels can be kept unmodulated by merging equal and opposite propagation phase with the geometric phase [28]. Fortunately, this approach also seems to obtain

switchable rational-multiple phase modulation by merging the suitable propagation phase value with geometric phase. The proposed approach can be used in several intriguing wavefront engineering applications, and it provides ease in design procedure when spin-switchable multiplicative or division operations are needed. Here, we explore two types of spin-switchable-metasurface-based designs. (1) Beam splitter/deflector: for input right circularly polarized (RCP) light, the designed metasurfaces will deflect the light, and by switching the input polarization to left circularly polarized (LCP) light, the same design will split the light at two different angles. (2) Rational-multiple spin-to-orbital angular momentum converter (SOC) designs: the rational complete phase-multiplication scheme facilitates a generalized scheme for spin-to-orbital angular momentum conversion that can switch any arbitrary premeditated OAM design to integer or fractional multiple OAM design by switching the polarization handedness of incident light. Our proposed approach, based on a non-interleaved metasurface, establishes a generalized principle for integer or fractional multiple of complete phase modulation and provides a new approach to realize several multifunctional wavefront engineering phenomena.

2. DESIGN PRINCIPLE

In general, for non-interleaved metasurfaces, the transmission matrix for the CP light can be written as $T = \begin{bmatrix} T_{RR} & T_{RL} \\ T_{LR} & T_{LL} \end{bmatrix}$. Here, T_{RR} and T_{LL} are the copolarization channels for LCP and RCP incoming light, respectively. T_{RL} and T_{LR} are the cross-polarizations for LCP and RCP light, respectively. In this work, cross-polarization channels are utilized for rational-multiple complete phase modulation. We use a C-2 rotational symmetric single silicon meta-atom on glass substrate and generalize the design principle, which can obtain the integer or fractional multiple complete phase modulation. It is known that the PB phase comes from the rotation $\theta(x, y)$ of dielectric/metallic nanostructures with respect to the x axis and imparts twice the rotational angle phase shift on transmitted cross-polarized light, i.e., $\mp 2\theta\sigma(x, y)$ when circularly polarized light ($\pm\sigma$) illuminates the sample at normal incidence as illustrated in Fig. 1. The operating wavelength $\lambda_o = 780$ nm, height of meta-atoms (H), and pitch are fixed for all the designs.

The expression for the Jones matrix, for the rotated meta-atom, for the incoming and transmitted electric fields can be written as [34]

$$J = R_c(\theta)\begin{bmatrix} e^{i\phi_{RR}} & e^{i\phi_{RL}} \\ e^{i\phi_{LR}} & e^{i\phi_{LL}} \end{bmatrix} R_c(-\theta) = \begin{bmatrix} e^{i\phi_{RR}} & e^{i(\phi_{RL}\pm 2\sigma\theta)} \\ e^{i(\phi_{LR}\mp 2\sigma\theta)} & e^{i\phi_{LL}} \end{bmatrix}, \quad (1)$$

where $R_c(\theta)$ is the rotation matrix; ϕ_{LL}, ϕ_{RL}, ϕ_{LR}, and ϕ_{RR} are propagation phases. For the RCP ($+\sigma$) input light, the expressions of PB phase for the cross-polarization transmission channel can be written as $\phi_{RCP\to LCP}(x, y) = -2\sigma\theta(x, y)$. Similarly, for the LCP ($-\sigma$) input light, the expressions of PB phase for the cross-polarization transmission channel can be written as $\phi_{LCP\to RCP}(x, y) = +2\sigma\theta(x, y)$. In addition to rotation an additional degree of freedom in terms of propagation/retardation phase, $\phi(x, y) = \phi_{LR} = \phi_{RL}$ can be introduced by spatially varying structural parameters L_1 and L_2. Therefore, $\phi_{RCP\to LCP}(x, y) = \phi(x, y) - 2\sigma\theta(x, y)$ and $\phi_{LCP\to RCP}(x, y) = \phi(x, y) + 2\sigma\theta(x, y)$ can be independently controlled by exploiting the $\phi(x, y)$ and $\theta(x, y)$ to achieve fractional or integer multiple complete phase modulation of factor m. For instance, $\phi(x, y) = \phi_{LL} = \phi_{RR} = \pm 4\theta(x, y)$ leads to $\phi_{RCP\to LCP}(x, y) = 2\theta/-6\theta$ and $\phi_{LCP\to RCP}(x, y) = 6\theta/-2\theta$, which indicates that 3 times of complete phase modulation can be imparted on left or right crossed CP light. For this scenario, in the case of RCP ($+\sigma = +1$) input light, the expression for transmitted electric field from Eq. (1) can be written as

$$E^{out}_{R_{in}} = \begin{bmatrix} e^{i\phi_{RR}} \\ e^{i(\phi_{LR}-2\theta=+4\theta-2\theta=2\theta)} \end{bmatrix} \text{ or } \begin{bmatrix} e^{i\phi_{RR}} \\ e^{i(\phi_{LR}-2\theta=-4\theta-2\theta=-6\theta)} \end{bmatrix}. \quad (2)$$

Similarly, in the case of LCP ($-\sigma = -1$) input light, the expression for transmitted electric field from Eq. (1) can be written as

$$E^{out}_{L_{in}} = \begin{bmatrix} e^{i(\phi_{RL}+2\theta=+4\theta+2\theta=6\theta)} \\ e^{i\phi_{LL}} \end{bmatrix} \text{ or } \begin{bmatrix} e^{i(\phi_{RL}+2\theta=-4\theta+2\theta=-2\theta)} \\ e^{i\phi_{LL}} \end{bmatrix}. \quad (3)$$

Figure 1 presents the schematic of metasurface design to achieve fractional or integer multiples of complete phase

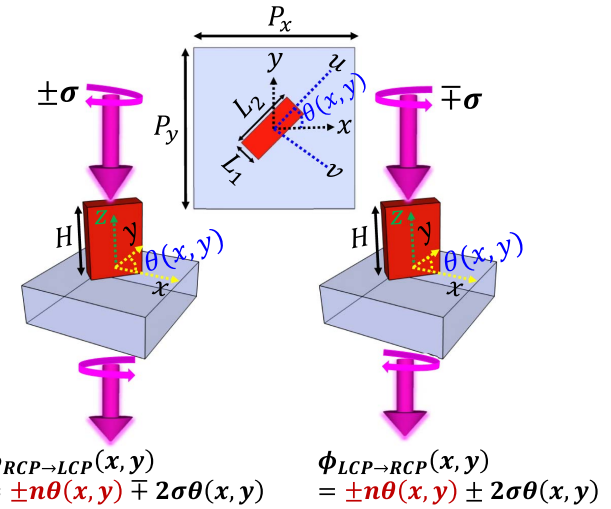

Fig. 1. Schematic illustration of a unit cell for rational-multiple phase modulation through merged propagation and geometric phases. For RCP ($\pm\sigma$) light, the silicon meta-atom of $H = 420$ nm rotated at $\theta(x, y)$ on glass substrate transfers a $\mp 2\sigma\theta(x, y)$ geometric phase shift on the cross-polarization channel, i.e., LCP ($\mp\sigma$) light (left side). The sign of the geometric phase gets reversed, i.e., $\pm 2\theta(x, y)$, while switching the input polarization, i.e., LCP ($\mp\sigma$) (right side). The propagation phase $\pm n\theta(x, y)$ can be merged with the PB phase, which yields to rational-multiple complete phase modulation on either RCP or LCP light. In the 2D representation (in the middle), $P_x = P_y = 400$ nm is the pitch of the unit cell, x and y are the global coordinates, u and v are the local coordinates of the meta-atom, $\theta(x, y)$ is the angle between u and x, and L_1 and L_2 are the spatially varying dimensions of the meta-atom. Herein, the additional parameters $+\sigma$ and $-\sigma$ are selected as right and left circular polarization, respectively.

modulation. It is illustrated that the expression for PB phase can be modified by adding/subtracting the propagation phase from the geometric phase, which can lead to spin-switchable rational-multiple complete phase modulation. It should be noted that, when propagation phase is added/subtracted from the PB phase, the global rational-multiple phase modulation w.r.t. initial phase in the same (when $n > 2$) or opposite direction (when $n < 2$) can be achieved on circularly crossed-polarized light by flipping the spin of incident light. The detailed explanation can be seen in Appendix A for the case of $\theta = \pi/8$. The value of multiplication factor m can be obtained on circularly crossed-polarized light upon switching the handedness of incident light by judiciously optimizing the $\phi(x, y)$ and $\theta(x, y)$. A generalized table is designed with incremental value n of propagation phase to achieve m times complete phase modulation on cross-polarization upon switching the handedness of polarization of incident light. The complete tabular illustration for different values of multiplication factor m is listed in Table 1. It is presented that by adding or subtracting the propagation phase from geometric phase, the global rational-multiple complete phase modulation can be achieved on the cross-polarization channel at output by flipping the polarization of incident light. One can interpret that the proposed approach provides several quick relationships to manipulate the CP orthogonal light, and it facilitates hassle-free parametric selection instead of building a bulk library when multiplication or division operations are needed. Here, numerical simulations are performed by the finite-difference time-domain (FDTD) Lumerical simulation tool, for normally incident CP light from the top of the meta-atom and the spatially variant structural parameters L_1 and L_2, and rotation angles $\theta(x, y)$ are optimized.

For high efficiency, along the complete phase modulation, uniform amplitude is an essential component. Thus, we carried out 2D parametric sweep between L_1 and L_2 for the fundamental unit cell. The amplitude and phase distributions of the fundamental meta-atom for the linearly orthogonal input polarization are shown in Fig. 2. Structural parameters with high amplitude are chosen in our designs for CP incident light.

3. SPIN-SELECTIVE BEAM DEFLECTOR AND SPLITTER

In the optical field, beam deflectors and beam splitters are well-established optical components, which can be realized by several techniques such as waveguides [35,36], gratings [37–39], and metamaterials [40–43]. Among them, metasurface-based beam steering devices are currently of great topical interest in research due to their subwavelength size, low fabrication cost, high efficiency, multifunctionality, and facile tunability. In recent years, metasurface-based multifunctional non-interleaved designs for beam splitting and deflection have been studied widely for linear and circular polarization. However, by using the propagation phase for linearly polarized light and PB phase for CP light, the transmitted beam splits/deflects at symmetrical angle due to fixed and opposite phase relationships between linearly/circularly orthogonal polarized light. For instance, Guo *et al.* proposed a single-layered metasurface design that splits and deflects the linearly polarized light at symmetrical angle by tuning the linearly polarized incident light [44]. Similarly, Wen *et al.* observed symmetric beam deflection for CP cross polarization by switching the spin of incident light [45]. Recent studies suggest that the fixed phase relationship

Table 1. A Generalized Tabular Representation of the Proposed Polarization-Switchable Rational-Multiple Complete-Phase-Modulation Scheme

Serial No.	Propagation/Structural/Retardation/Dynamic Phase and Geometric Phase	Phase Modulation
1	$\phi_{RCP\to LCP}(x,y) = 0 - 2\theta(x,y) = -2\theta(x,y)$ $\phi_{LCP\to RCP}(x,y) = 0 + 2\theta(x,y) = 2\theta(x,y)$	Equal with opposite sign
2	$\phi_{RCP\to LCP}(x,y) = \pm 0.4\theta(x,y) - 2\theta(x,y) = -1.6\theta(x,y)/-2.4\theta(x,y)$ $\phi_{LCP\to RCP}(x,y) = \pm 0.4\theta(x,y) + 2\theta(x,y) = 2.4\theta(x,y))/1.6\theta(x,y)$	1.5× with opposite sign
3	$\phi_{RCP\to LCP}(x,y) = \pm\theta(x,y) - 2\theta(x,y) = -\theta(x,y)/-3\theta(x,y)$ $\phi_{LCP\to RCP}(x,y) = \pm\theta(x,y) + 2\theta(x,y) = 3\theta(x,y))/\theta(x,y)$	3× with opposite sign
4	$\phi_{RCP\to LCP}(x,y) = \pm 2\theta(x,y) - 2\theta(x,y) = 0(x,y)/-4\theta(x,y)$ $\phi_{LCP\to RCP}(x,y) = \pm 2\theta(x,y) + 2\theta(x,y) = 4\theta(x,y))/0(x,y)$	0×
5	$\phi_{RCP\to LCP}(x,y) = \pm 2.5\theta(x,y) - 2\theta(x,y) = 0.5\theta(x,y)/-4.5\theta(x,y)$ $\phi_{LCP\to RCP}(x,y) = \pm 2.5\theta(x,y) + 2\theta(x,y) = 4.5\theta(x,y))/-0.5\theta(x,y)$	9×
6	$\phi_{RCP\to LCP}(x,y) = \pm 3\theta(x,y) - 2\theta(x,y) = \theta(x,y)/-5\theta(x,y)$ $\phi_{LCP\to RCP}(x,y) = \pm 3\theta(x,y) + 2\theta(x,y) = 5\theta(x,y))/-\theta(x,y)$	5×
7	$\phi_{RCP\to LCP}(x,y) = \pm 4\theta(x,y) - 2\theta(x,y) = 2\theta(x,y)/-6\theta(x,y)$ $\phi_{LCP\to RCP}(x,y) = \pm 4\theta(x,y) + 2\theta(x,y) = 6\theta(x,y))/-2\theta(x,y)$	3×
8	$\phi_{RCP\to LCP}(x,y) = \pm 4.67\theta(x,y) - 2\theta(x,y) = 2.67\theta(x,y)/-6.67\theta(x,y)$ $\phi_{LCP\to RCP}(x,y) = \pm 4.67\theta(x,y) + 2\theta(x,y) = 6.67\theta(x,y))/-2.67\theta(x,y)$	~2.5×
9	$\phi_{RCP\to LCP}(x,y) = \pm 6\theta(x,y) - 2\theta(x,y) = 4\theta(x,y)/-8\theta(x,y)$ $\phi_{LCP\to RCP}(x,y) = \pm 6\theta(x,y) + 2\theta(x,y) = 8\theta(x,y))/-4\theta(x,y)$	2×
10	$\phi_{RCP\to LCP}(x,y) = \pm 10\theta(x,y) - 2\theta(x,y) = 8\theta(x,y)/-12\theta(x,y)$ $\phi_{LCP\to RCP}(x,y) = \pm 10\theta(x,y) + 2\theta(x,y) = 12\theta(x,y))/-8\theta(x,y)$	1.5×

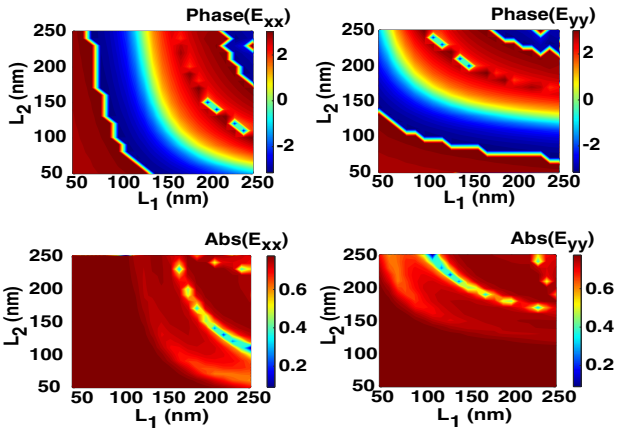

Fig. 2. Amplitude and phase distribution of the fundamental unit cell for the linearly orthogonal input polarizations. From electric fields E_{xx} and E_{yy}, the transmission amplitude (top) and phase (bottom) are obtained from parametric sweep of L_1 and L_2 ranging from 50 to 250 nm. These results indicate the high amplitude as well as complete 2π phase coverage at operating frequency.

can be modified for CP orthogonal polarization by merging the propagation phase with geometric phase [26]. By using hybrid phase modulation Wang *et al.* [28] and Li *et al.* [27] proposed that asymmetric deflection can be realized for the CP light. However, to the best of our knowledge, there is a lack of single-layered non-interleaved design that can perform beam deflection for one CP light in a certain direction, and the same design has the tendency to split the light symmetrically for the other CP light. Fortunately, the proposed rational-multiple complete modulation scheme has the potential to realize a bifunctional design to perform the said functionalities in a handy way. The schematic of the bifunctional beam steering design is illustrated in Fig. 3. It can be inferred that under the incidence of RCP light, the designed metasurfaces can be regarded as a beam deflector, while the designed device acts as a beam splitter under the LCP light.

To implement the proposed design, $\phi(x,y) = +6\theta(x,y)$ is set for propagation phase; therefore, $\phi_{\mathrm{RCP}\to\mathrm{LCP}}(x,y) = 4\theta$ and $\phi_{\mathrm{LCP}\to\mathrm{RCP}}(x,y) = 8\theta$, which indicates that twice the complete phase modulation can be achieved by switching the incident polarization. After optimizing the L_1 and L_2 and $\theta(x,y)$, we arrange four meta-atoms in the supercell with phase difference of $\pi/2$ w.r.t neighbouring elements for the RCP input light as illustrated in Fig. 3 (left side), and then the design works as a beam deflector according to the generalized Snell's law [1]. The structural parametric values of meta-atoms selected for the beam deflector are tabulated in Table 2, and they are arranged periodically from left to right as shown in Fig. 3. The analytical beam deflection according to the generalized Snell's law can be calculated as

$$\sin(\theta_t)n_t - \sin(\theta_i)n_i = \frac{\lambda_0}{2\pi}\frac{d\phi}{dx} = \frac{\lambda_0}{2\pi}\frac{2\pi}{dx},$$
$$\theta_t = |\theta_t| = \arcsin\left(\frac{\lambda_o}{n_t\Lambda}\right) = \arcsin\left(\frac{780\ \mathrm{nm}}{1.45\times 1600\ \mathrm{nm}}\right) = 19.64°. \quad (4)$$

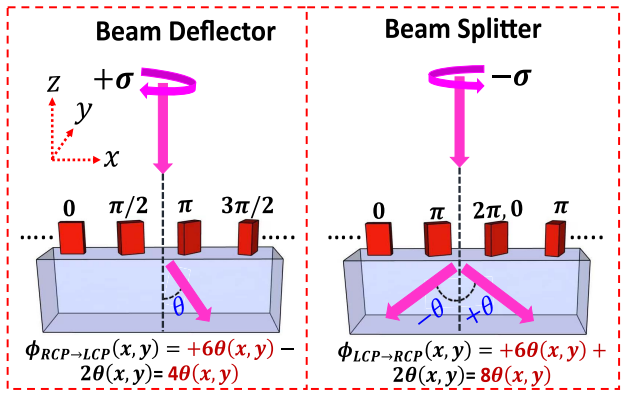

Fig. 3. Design and operating principle of spin-selective beam deflector and splitter. For RCP $(+\sigma)$ incident light, the structural parameters are obtained when propagation phase $\phi(x,y) = +6\theta(x,y)$ is combined with geometric phase and meta-atoms are arranged in a super-cell with the phase difference of $\pi/2$ (left side). This design works as beam deflector that deflects cross-polarized light at a certain angle θ. For the LCP $(-\sigma)$, twice the phase multiplication with each of meta-atoms (excluding the fundamental one) turns the unit cells into binary unit cells with phase delay of π, which splits the light (right side).

Table 2. Structural and Rotational Parametric Values of Selected Meta-Atoms for the Beam Deflector/Splitter

Meta-atom No.	L_1 (nm)	L_2 (nm)	$\theta(x,y)$
1	180	90	0
2	195	130	$\pi/8$
3	120	185	$\pi/4$
4	175	110	$3\pi/8$

In Eq. (4), n_i (air) $= 1$, $n_t = 1.45$ (glass substrate), and the period of the supercell Λ = pitch × amount of elements = 400 nm × 4 = 1600 nm are selected. The above equation indicates that the array of periodically arranged meta-atoms covering 0–2π complete phase shift deflects the incident light at 19.64°.

Interestingly, for the LCP input light, each element in the supercell (excluding the fundamental one) experiences twice the phase shift. Therefore, the phase difference between the neighboring elements will be π. Technically, one can state that binary phase gradient $\frac{d\phi}{dx}$ is placed periodically on the metasurface. Hence, the designed device works as a beam splitter again according to the generalized Snell's law [42]:

$$\sin(\theta_t)n_t - \sin(\theta_i)n_i = \frac{\lambda_0}{2\pi}\frac{d\phi}{dx} = \frac{\lambda_0}{2\pi}\frac{\pm\pi}{dx},$$
$$\theta_t = \arcsin\frac{\lambda_0}{2\pi\times n_t}\frac{\pm\pi}{dx} = \arcsin\left(\frac{780}{2\pi\times 1.45}\frac{\pm\pi}{400}\right)$$
$$= \pm 42.25°. \quad (5)$$

In Eq. (5), n_i (air) $= 1$ and $n_t = 1.45$ (glass substrate) are set. The above equation indicates that transmitted light will bend at two different angles, i.e., ±42.25°.

The FDTD simulation results of 10 periodically arranged supercells for beam deflection and splitting are presented in

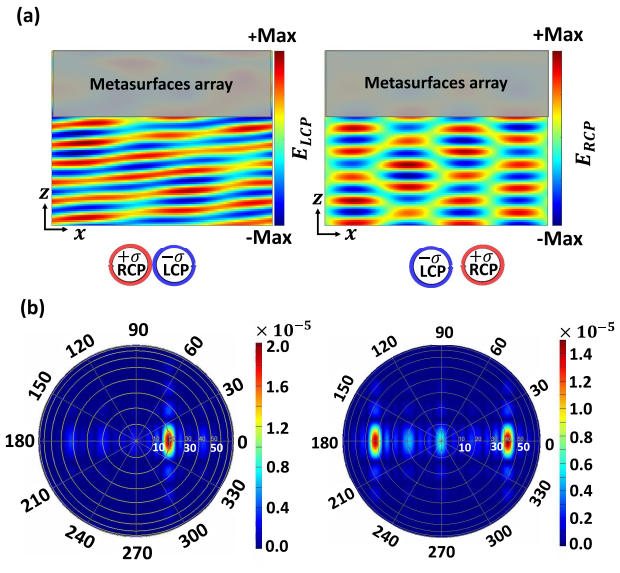

Fig. 4. Numerically computed results for beam deflection and splitting. (a) Under the incidence of RCP and LCP light on the meta design, the transmitted electric fields E_{LCP} (left side) and E_{LCP} (right side) after passing through metasurface array in the x–z plane clearly demonstrate the polarization-switchable beam deflection and splitting phenomena. (b) Far-field results of spin-selective beam deflector and splitter. The circularly cross-polarized light deflects under RCP incidence and splits under LCP incidence. The left arrow in the middle indicates incident polarization, and the right arrow indicates the polarization handedness at output.

Fig. 4. The Fig. 4(a) (left side) shows that the wavefront of E_{LCP} will refract from the normal at a certain angle under RCP light. The disturbance of uniformity of transmitted electric field E_{RCP} under LCP light shows that the beam is splitting at certain angles (right side). The far-field distribution results are included in Fig. 4(b), which show that strong beam deflection and splitting can be observed in the desired direction. It is worth mentioning that the deflection and splitting angles computed by FDTD simulations exactly match with the analytically calculated results.

4. SPIN-SWITCHABLE RATIONAL-MULTIPLE SOC DESIGNS

A vortex beam (VB) is a spiral distribution of EM wavefront that carries OAM determined by an azimuthal phase term $\exp(i\ell\phi)$, where ℓ is a topological charge and ϕ is the azimuthal phase angle. VBs can be used in several applications such as optical tweezers, quantum information coding, signal processing, and OAM communication [46–50]. Optics has seen sudden progress in metasurface-based VB generation through SOC and OAM-state manipulation both in free space and on a chip [8,13,13,32,51]. OAM-based optical communication and high-dimensional quantum information systems demand the performance of complex switching and routing [46].

Here, we also explore the versatility of the proposed generalized rational-multiple complete-phase-modulation scheme for SOC designs, which generates two beams for circularly orthogonal polarization with the value of topological charge ℓ_1 and $\ell_2 = m\ell_1$. The value of m can be obtained by suitable selection of modified PB phase expression as presented in Table 1. Complex switching operations such as $m\ell$ including even (2ℓ) and odd ($2\ell \pm 1$) require the rational multiplication of the OAM mode with factor m, which can be useful in fiber-optic mode conversion and optical data encoding. Our proposed spin-dependent phase-multiplication method has the potential to perform these operations with the predesigned metasurface producing arbitrary value of ℓ at output as presented in Fig. 5.

The schematic of spin-switchable SOC design in Fig. 5 illustrates that for the RCP input light, a metasurface can be designed that can carry OAM with an arbitrary value of topological charge ℓ_1 on transmitted cross-polarization channel. On switching the handedness of input light, i.e., LCP, the predesigned metasurface can multiply the OAM mode with any integer or fraction value of multiplication factor m on the cross-polarization channel at output depending upon the design feature. To achieve polarization-switchable rational-multiple OAM mode conversion, we implemented five different designs for RCP input light. Among them, the first four designs can multiply the OAM mode with topological charge value $\ell_1 = 2$ with multiplication factor value $m = 1.5$, $m = 2$, $m \approx 2.5$, $m = 3$, and the fifth design can multiply the OAM mode with topological charge value $\ell_1 = -2$ with multiplication factor value $m = -3$ upon switching the input polarization handedness. The spatially varying structural parameters L_1 and L_2 of meta-atoms and rotation angels $\theta(x, y)$ for each of the designs are optimized separately. The total phase distribution ϕ_{total} of meta-atoms on the substrate can be calculated by $\phi_{\mathrm{total}}(\alpha, r) = \alpha\phi_\ell(r)$, where α and r are the coordinate parameters in the polar coordinates system. $\phi_\ell(r)$ is the phase distribution of the arbitrary value of topological charge ℓ.

To perform switchable rational-multiple SOC, five types of metasurface designs are numerically simulated. For each of the five designs, the meta-atoms are arranged on the glass substrate such that each device transmits LCP light carrying topological

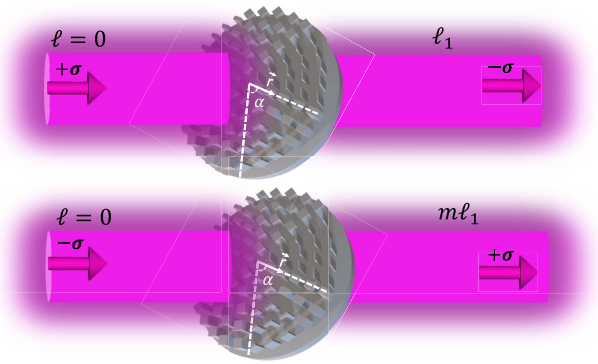

Fig. 5. Schematic of the working principle of the rational-multiple spin-switchable SOC. For RCP incoming light, the LCP light emerging from the back side of the design can carry OAM with any arbitrary value of topological charge value ℓ. By switching the incident light to LCP, the predesigned device can switch the topological charge value multiple of m depending upon the design feature. In this representation, the design is composed of silicon meta-atoms with azimuthal angle α and radius r on the glass substrate.

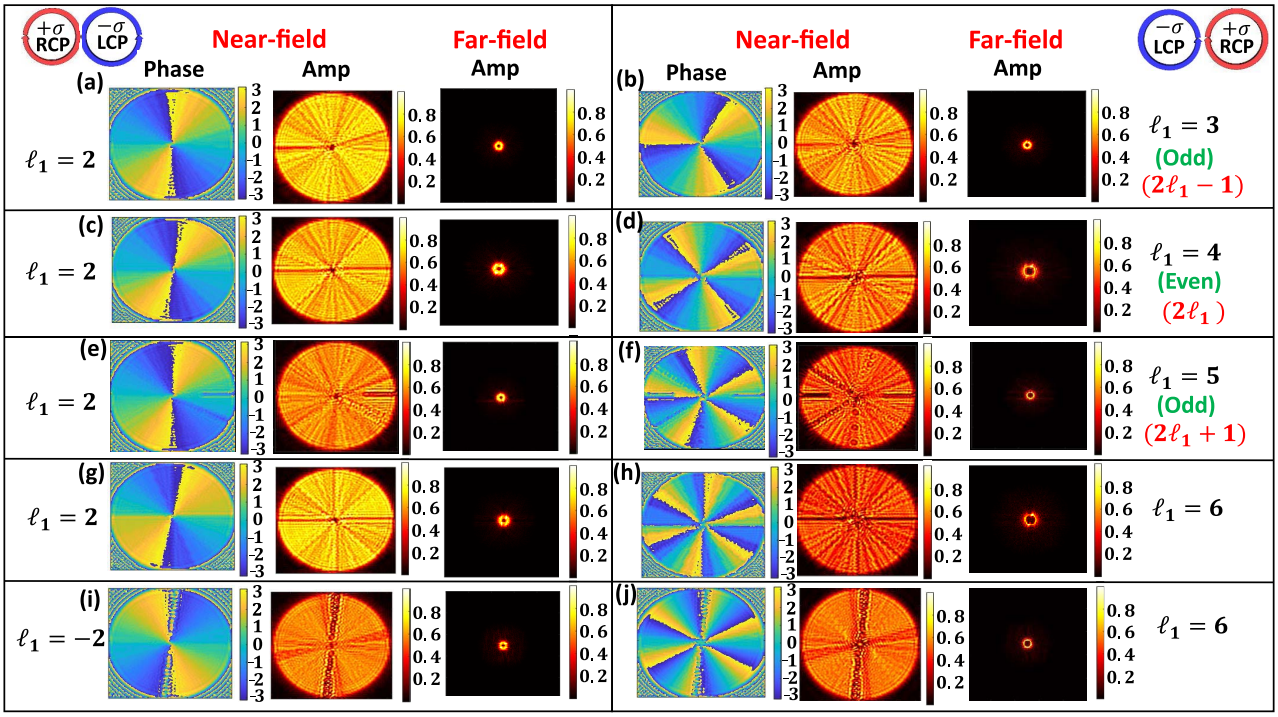

Fig. 6. Numerical simulation results for polarization-switchable rational-multiple SOC designs. Five different designs with different structural parameters for OAM mode with topological charge value $\ell_1 = 2$ are implemented; the specific design can switch to 1.5, 2, 2.5, 3, or −3 times of ℓ_1 by switching the handedness of incident light. (a), (c), (e), (g), (i) Near-field amplitude and phase of each design and far-field result of each design; (b), (d), (f), (h), (j) their corresponding rational-multiple results.

charge of value $\ell_1 = 2$ for the RCP incoming light [Figs. 6(a), 6(c), 6(e), and 6(g)], except the fifth design, which carries OAM value $\ell_1 = -2$ [Fig. 6(i)]. For LCP input light, these designs are encoded such that they can perform odd $-\ell_1(2\ell_1 - 1)$ [Fig. 6(b)], even $-\ell_1(2\ell_1)$ [Fig. 6(d)], odd $-\ell_1(2\ell_1 + 1)$ [Fig. 6(f)], $m\ell_1$ where $m = 3$ [Fig. 6(h)], and $m\ell_1 = m \times (-2)$ where $m = -3$ [Fig. 6(j)]. These operations are performed by multiplication of ℓ_1 with multiplication factors $m = 1.5$, $m = 2$, $m = 2.5$, $m = 3$, and $m = -3$ obtained from a hybrid phase-modulation scheme (Table 1). Conversely, it can be asserted that for RCP light, each design is performing division operation on the transmitted cross-polarized light, i.e., LCP such that $\ell_1 = \ell_2/1.5 = 3/1.5 = 2$ [Fig. 6(a)], $\ell_1 = \ell_2/2 = 4/2 = 2$ [Fig. 6(c)], $\ell_1 = \ell_2/2 = 5/2.5 = 2$ [Fig. 6(e)], $\ell_1 = \ell_2/3 = 6/3 = 2$ [Fig. 6(g)], and $\ell_1 = \ell_2/3 = -6/3 = -2$ [Fig. 6(i)]. The radius r of simulated designs is 21.1 μm. The near-field and far-field results of each of the five designs are presented in Fig. 6. The near-field phase profile of each design demonstrates the mode conversion with multiplication factor. In the far field, doughnut shapes of the amplitude also validate the rational-multiple OAM mode conversion.

5. ROUTES TO REALIZE THE PROPOSED DESIGNS EXPERIMENTALLY

All of the above mentioned designs can be validated experimentally by following the processes reported in Refs. [22,28,52–54], which have been experimentally realized, having silicon meta-atoms on the glass substrate at the same operating frequency region with almost the same pitch and height of meta-atoms for holography and beam deflection applications. The fabrication process starts with the deposition of a silicon layer through plasma-enhanced chemical vapor deposition with subsequent deposition of metallic film through electron beam evaporation, which works as a hard mask. After that, positive resist coating is needed to pattern the structures through electron beam lithography, and subsequent etching of written silicon needs to be performed through inductive etching. In the end, the additional metal needs to be removed through etchant. After successful fabrication, the standard optical setup utilized in Refs. [13,22] can be arranged for optical measurements.

6. CONCLUSION

In summary, by simultaneous exploitation of propagation and geometric phases, a generalized scheme is proposed for rational-multiple complete phase modulation. Two types of designs, including spin-selective beam deflector/splitter and spin-switchable SOC designs, are numerically validated. The spin-selective beam deflector/splitter design works as beam deflector for RCP light and turns into a beam splitter under LCP input light. The SOC designs tend to convert any predesigned arbitrary OAM value to a rational-multiple OAM value on circularly orthogonal polarization by switching the incidence polarization. It is predicted that the proposed design scheme will empower a broad range of metasurface-based applications

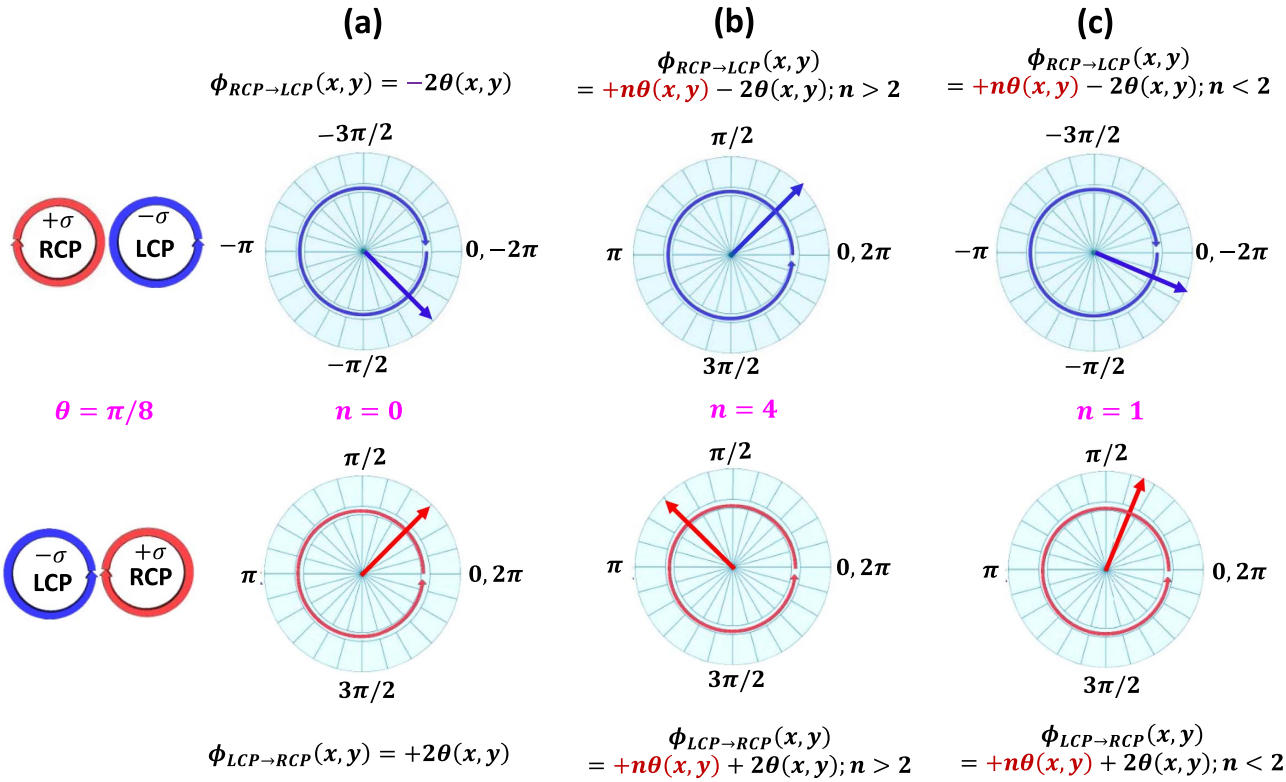

Fig. 7. Phase modulations when the meta-atom is rotated at $\theta = \pi/8$. (a) The PB phase provides equal phase modulation with opposite sign; (b) 3 times phase modulation when $n = 4$, and (c) 3 times phase modulation with opposite sign when $n = 1$.

such as imaging, sensing, quantum science, and optical communication.

APPENDIX A: EXPLANATION OF RATIONAL MULTIPLICATION FOR DIFFERENT PROPAGATION PHASE VALUES WHEN $\theta = \pi/8$

Figures 7(a)–7(c) depict the phase modulation under RCP (top) and LCP (bottom) incidence polarization when the propagation phase with $n = 0$, $n > 2$, and $n < 2$ is merged with geometric phase and the value of rotation angle is $\theta \geq 0$. When a meta-atom is rotated at $\theta = \pi/8$, the PB phase value $-\pi/4$ in the clockwise (CW) direction can be obtained for the cross-polarized light, i.e., LCP under RCP incidence [Fig. 7(a) (top)]. The cross-polarized, i.e., RCP light, experiences equal phase shift, i.e., $\pi/4$, in the counter-clockwise (CCW) direction by flipping the incident light polarization to LCP [Fig. 7(a) (bottom)]. When the propagation phase value $n\theta = 4 \times \pi/8 = \pi/2$ is added to PB phase, the transmitted cross polarization, i.e., LCP, will have phase value $\pi/4$ in the CCW direction [Fig. 7(b) (top)]. On transmitted cross-polarized light, 3 times the phase shift, i.e., $3\pi/4$, can be obtained in the CCW direction by switching the handedness of incident polarization to LCP [Fig. 7(b) (bottom)]. When the propagation phase value $n\theta = 1 \times \pi/8 = \pi/8$ is added to PB phase, the transmitted cross polarization, i.e., LCP, will have phase value $-\pi/8$ in the CW direction [Fig. 7(c) (top)]. On transmitted cross-polarized light, 3 times the phase shift, i.e., $3\pi/8$, can be obtained in the CCW direction by switching the handedness of incident polarization to LCP [Fig. 7(c) (bottom)]. There will be no phase shift on transmitted cross LCP light when propagation phase $n\theta = 2 \times \pi/8 = \pi/4$; see Ref. [28].

Funding. Shenzhen University Starting Fund (2019073); National Natural Science Foundation of China (61905147, 61935013, 91750205, U1701661); Leading Talents Program of Guangdong Province (00201505, 2019JC01Y178); Natural Science Foundation of Guangdong Province (2016A030312010, 2019TQ05X750, 2020A1515010598); Science, Technology and Innovation Commission of Shenzhen Municipality (JCYJ20180507182035270, KQTD2017033011044403, KQTD20180412181324255).

Acknowledgment. The authors acknowledge the technical support from the Nanophotonics Research Center of Shenzhen university.

Disclosures. The authors declare no competing financial interests.

Data Availability. Data underlying the results presented in this paper are not publicly available at this time but may be obtained from the authors upon reasonable request.

†These authors contributed equally to this work.

REFERENCES

1. N. Yu, P. Genevet, M. A. Kats, F. Aieta, J. P. Tetienne, F. Capasso, and Z. Gaburro, "Light propagation with phase discontinuities: generalized laws of reflection and refraction," Science **334**, 333–337 (2011).
2. N. Yu and F. Capasso, "Flat optics with designer metasurfaces," Nat. Mater. **13**, 139–150 (2014).
3. D. Wen, F. Yue, G. Li, G. Zheng, K. Chan, S. Chen, M. Chen, K. F. Li, P. W. H. Wong, K. W. Cheah, E. Y. B. Pun, S. Zhang, and X. Chen, "Helicity multiplexed broadband metasurface holograms," Nat. Commun. **6**, 8241 (2015).
4. A. U. R. Khalid, J. Liu, Y. Han, N. Ullah, R. Zhao, and Y. Wang, "Multichannel polarization encoded reflective metahologram using VO_2 spacer in visible regime," Opt. Commun. **451**, 211–215 (2019).
5. Y. Hu, L. Li, Y. Wang, M. Meng, L. Jin, X. Luo, Y. Chen, X. Li, S. Xiao, H. Wang, Y. Luo, C. W. Qiu, and H. Duan, "Trichromatic and tripolarization-channel holography with noninterleaved dielectric metasurface," Nano Lett. **20**, 994–1002 (2020).
6. G. Zheng, H. Mühlenbernd, M. Kenney, G. Li, T. Zentgraf, and S. Zhang, "Metasurface holograms reaching 80% efficiency," Nat. Nanotechnol. **10**, 308–312 (2015).
7. L. Jin, Z. Dong, S. Mei, Y. F. Yu, Z. Wei, Z. Pan, S. D. Rezaei, X. Li, A. I. Kuznetsov, Y. S. Kivshar, J. K. W. Yang, and C.-W. Qiu, "Noninterleaved metasurface for (2^6-1) spin-and wavelength-encoded holograms," Nano Lett. **18**, 8016–8024 (2018).
8. L. Jin, Y.-W. Huang, Z. Jin, R. C. Devlin, Z. Dong, S. Mei, M. Jiang, W. T. Chen, Z. Wei, H. Liu, J. Teng, A. Danner, X. Li, S. Xiao, S. Zhang, C. Yu, J. K. W. Yang, F. Capasso, and C.-W. Qiu, "Dielectric multi-momentum meta-transformer in the visible," Nat. Commun. **10**, 4789 (2019).
9. Y. Bao, J. Yan, X. Yang, C.-W. Qiu, and B. Li, "Point-source geometric metasurface holography," Nano Lett. **21**, 2332–2338 (2020).
10. K. Huang, Z. Dong, S. Mei, L. Zhang, Y. Liu, H. Liu, H. Zhu, J. Teng, B. Luk'yanchuk, J. K. Yang, and C.-W. Qiu, "Silicon multi-meta-holograms for the broadband visible light," Laser Photon. Rev. **10**, 500–509 (2016).
11. P. Yu, J. Li, X. Li, G. Schütz, M. Hirscher, S. Zhang, N. Liu, and S. Liu, "Generation of switchable singular beams with dynamic metasurfaces," ACS Nano **13**, 7100–7106 (2019).
12. J. Yang, H. Zhou, and T. Lan, "All-dielectric reflective metasurface for orbital angular momentum beam generation," Opt. Mater. Express **9**, 3594–3603 (2019).
13. R. C. Devlin, A. Ambrosio, N. A. Rubin, J. P. B. Mueller, and F. Capasso, "Arbitrary spin-to-orbital angular momentum conversion of light," Science **358**, 896–901 (2017).
14. E. Arbabi, A. Arbabi, S. M. Kamali, Y. Horie, and A. Faraon, "Multiwavelength polarization-insensitive lenses based on dielectric metasurfaces with meta-molecules," Optica **3**, 628–633 (2016).
15. V. Sanjeev, Z. Shi, F. Capasso, E. Lee, A. Y. Zhu, W. T. Chen, and M. Khorasaninejad, "A broadband achromatic metalens for focusing and imaging in the visible," Nat. Nanotechnol. **13**, 220–226 (2017).
16. W. T. Chen, A. Y. Zhu, J. Sisler, Z. Bharwani, and F. Capasso, "A broadband achromatic polarization-insensitive metalens consisting of anisotropic nanostructures," Nat. Commun. **10**, 355 (2019).
17. M. Khorasaninejad, A. Y. Zhu, C. Roques-Carmes, W. T. Chen, J. Oh, I. Mishra, R. C. Devlin, and F. Capasso, "Polarization-insensitive metalenses at visible wavelengths," Nano Lett. **16**, 7229–7234 (2016).
18. H. Yang, G. Li, X. Su, G. Cao, Z. Zhao, X. Chen, and W. Lu, "Reflective metalens with sub-diffraction-limited and multifunctional focusing," Sci. Rep. **7**, 12632 (2017).
19. Z. Li, P. Lin, Y.-W. Huang, J.-S. Park, W. T. Chen, Z. Shi, C.-W. Qiu, J.-X. Cheng, and F. Capasso, "Meta-optics achieves RGB-achromatic focusing for virtual reality," Sci. Adv. **7**, eabe4458 (2021).
20. T. Shi, Y. Wang, Z. L. Deng, X. Ye, Z. Dai, Y. Cao, B. O. Guan, S. Xiao, and X. Li, "All-dielectric kissing-dimer metagratings for asymmetric high diffraction," Adv. Opt. Mater. **7**, 1901389 (2019).
21. G. Li, S. Chen, N. Pholchai, B. Reineke, P. W. H. Wong, E. Y. B. Pun, K. W. Cheah, T. Zentgraf, and S. Zhang, "Continuous control of the nonlinearity phase for harmonic generations," Nat. Mater. **14**, 607–612 (2015).
22. B. Reineke, B. Sain, R. Zhao, L. Carletti, B. Liu, L. Huang, C. De Angelis, and T. Zentgraf, "Silicon metasurfaces for third harmonic geometric phase manipulation and multiplexed holography," Nano Lett. **19**, 6585–6591 (2019).
23. E. Almeida, O. Bitton, and Y. Prior, "Nonlinear metamaterials for holography," Nat. Commun. **7**, 12533 (2016).
24. W. Ye, F. Zeuner, X. Li, B. Reineke, S. He, C. W. Qiu, J. Liu, Y. Wang, S. Zhang, and T. Zentgraf, "Spin and wavelength multiplexed nonlinear metasurface holography," Nat. Commun. **7**, 11930 (2016).
25. C. Schlickriede, N. Waterman, B. Reineke, P. Georgi, G. Li, S. Zhang, and T. Zentgraf, "Imaging through nonlinear metalens using second harmonic generation," Adv. Mater. **30**, 1703843 (2018).
26. J. P. B. Mueller, N. A. Rubin, R. C. Devlin, B. Groever, and F. Capasso, "Metasurface polarization optics: independent phase control of arbitrary orthogonal states of polarization," Phys. Rev. Lett. **118**, 113901 (2017).
27. S. Li, X. Li, G. Wang, S. Liu, L. Zhang, C. Zeng, L. Wang, Q. Sun, W. Zhao, and W. Zhang, "Multidimensional manipulation of photonic spin Hall effect with a single-layer dielectric metasurface," Adv. Opt. Mater. **7**, 1801365 (2019).
28. B. Wang, F. Dong, H. Feng, D. Yang, Z. Song, L. Xu, W. Chu, Q. Gong, and Y. Li, "Rochon-prism-like planar circularly polarized beam splitters based on dielectric metasurfaces," ACS Photon. **5**, 1660–1664 (2017).
29. P. Huo, C. Zhang, W. Zhu, M. Liu, S. Zhang, S. Zhang, L. Chen, H. J. Lezec, A. Agrawal, Y. Lu, and T. Xu, "Photonic spin-multiplexing metasurface for switchable spiral phase contrast imaging," Nano Lett. **20**, 2791–2798 (2020).
30. T. Li, X. Xu, B. Fu, S. Wang, B. Li, Z. Wang, and S. Zhu, "Integrating the optical tweezers and spanner onto an individual single-layer metasurface," Photon. Res. **9**, 1062–1068 (2021).
31. K. Zhang, Y. Yuan, X. Ding, H. Li, B. Ratni, Q. Wu, J. Liu, S. N. Burokur, and J. Tan, "Polarization-engineered noninterleaved metasurface for integer and fractional orbital angular momentum multiplexing," Laser Photon. Rev. **15**, 2000351 (2021).
32. Y. Guo, S. Zhang, M. Pu, Q. He, J. Jin, M. Xu, Y. Zhang, P. Gao, and X. Luo, "Spin-decoupled metasurface for simultaneous detection of spin and orbital angular momenta via momentum transformation," Light Sci. Appl. **10**, 63 (2021).
33. K. Zhang, Y. Yuan, X. Ding, B. Ratni, S. N. Burokur, and Q. Wu, "High-efficiency metalenses with switchable functionalities in microwave region," ACS Appl. Mater. Interfaces **11**, 28423–28430 (2019).
34. C. Chen, S. Gao, X. Xiao, X. Ye, S. Wu, W. Song, H. Li, S. Zhu, and T. Li, "Highly efficient metasurface quarter-wave plate with wave front engineering," Adv. Photon. Res. **2**, 2000154 (2021).
35. X. Gao, J. H. Shi, X. Shen, H. F. Ma, W. X. Jiang, L. Li, and T. J. Cui, "Ultrathin dual-band surface plasmonic polariton waveguide and frequency splitter in microwave frequencies," Appl. Phys. Lett. **102**, 151912 (2013).
36. T. E. Schlesinger, Y. Chiu, D. D. Stancil, and R. S. Burton, "Design and simulation of waveguide electrooptic beam deflectors," J. Lightwave Technol. **13**, 2049–2052 (1995).
37. Z. Wang, Y. Tang, L. Wosinski, and S. He, "Experimental demonstration of a high efficiency polarization splitter based on a one-dimensional grating with a Bragg reflector underneath," IEEE Photon. Technol. Lett. **22**, 1568–1570 (2010).
38. J. Feng and Z. Zhou, "Polarization beam splitter using a binary blazed grating coupler," Opt. Lett. **32**, 1662–1664 (2007).
39. X. Wang, D. Wilson, R. Muller, P. Maker, and D. Psaltis, "Liquid-crystal blazed-grating beam deflector," Appl. Opt. **39**, 6545–6555 (2000).
40. Z. Zhou, J. Li, R. Su, B. Yao, H. Fang, K. Li, L. Zhou, J. Liu, D. Stellinga, C. P. Reardon, T. F. Krauss, and X. Wang, "Efficient silicon metasurfaces for visible light," ACS Photon. **4**, 544–551 (2017).
41. D. Zhang, M. Ren, W. Wu, N. Gao, X. Yu, W. Cai, X. Zhang, and J. Xu, "Nanoscale beam splitters based on gradient metasurfaces," Opt. Lett. **43**, 267–270 (2018).
42. A. Ozer, N. Yilmaz, H. Kocer, and H. Kurt, "Polarization-insensitive beam splitters using all-dielectric phase gradient metasurfaces at visible wavelengths," Opt. Lett. **43**, 4350–4353 (2018).

43. S. Kita, K. Takata, M. Ono, K. Nozaki, E. Kuramochi, K. Takeda, and M. Notomi, "Coherent control of high efficiency metasurface beam deflectors with a back partial reflector," APL Photon. **2**, 46104 (2017).
44. Z. Guo, L. Zhu, K. Guo, F. Shen, and Z. Yin, "High-order dielectric metasurfaces for high-efficiency polarization beam splitters and optical vortex generators," Nanoscale Res. Lett. **12**, 512 (2017).
45. D. Wen, F. Yue, S. Kumar, Y. Ma, M. Chen, X. Ren, P. E. Kremer, B. D. Gerardot, M. R. Taghizadeh, G. S. Buller, and X. Chen, "Metasurface for characterization of the polarization state of light," Opt. Express **23**, 10272–10281 (2015).
46. Y. Wen, I. Chremmos, Y. Chen, Y. Zhang, and S. Yu, "Arbitrary multiplication and division of the orbital angular momentum of light," Phys. Rev. Lett. **124**, 213901 (2020).
47. G. Ruffato, M. Massari, and F. Romanato, "Multiplication and division of the orbital angular momentum of light with diffractive transformation optics," Light Sci. Appl. **8**, 113 (2019).
48. Y. Shen, X. Wang, Z. Xie, C. Min, X. Fu, Q. Liu, M. Gong, and X. Yuan, "Optical vortices 30 years on: OAM manipulation from topological charge to multiple singularities," Light Sci. Appl. **8**, 90 (2019).
49. J. Wang, J. Y. Yang, I. M. Fazal, N. Ahmed, Y. Yan, H. Huang, Y. Ren, Y. Yue, S. Dolinar, M. Tur, and A. E. Willner, "Terabit free-space data transmission employing orbital angular momentum multiplexing," Nat. Photonics **6**, 488–496 (2012).
50. A. E. Willner, H. Huang, Y. Yan, Y. Ren, N. Ahmed, G. Xie, C. Bao, L. Li, Y. Cao, Z. Zhao, J. Wang, M. P. J. Lavery, M. Tur, S. Ramachandran, A. F. Molisch, N. Ashrafi, and S. Ashrafi, "Optical communications using orbital angular momentum beams," Adv. Opt. Photon. **7**, 66 (2015).
51. Z. Jin, D. Janoschka, J. Deng, L. Ge, P. Dreher, B. Frank, G. Hu, J. Ni, Y. Yang, J. Li, C. Yu, D. Lei, G. Li, S. Xiao, S. Mei, H. Giessen, F. Meyer zu Heringdorf, and C.-W. Qiu, "Phyllotaxis-inspired nanosieves with multiplexed orbital angular momentum," eLight **1**, 5 (2021).
52. R. Zhao, B. Sain, Q. Wei, C. Tang, X. Li, L. Huang, Y. Wang, and T. Zentgraf, "Multichannel vectorial holographic display and encryption," Light Sci. Appl. **7**, 95 (2018).
53. Q. Wang, E. Plum, Q. Yang, X. Zhang, Q. Xu, Y. Xu, J. Han, and W. Zhang, "Reflective chiral meta-holography: multiplexing holograms for circularly polarized waves," Light Sci. Appl. **7**, 2047–7538 (2018).
54. Q.-T. Li, F. Dong, B. Wang, F. Gan, J. Chen, Z. Song, L. Xu, W. Chu, Y.-F. Xiao, Q. Gong, and Y. Li, "Polarization-independent and high-efficiency dielectric metasurfaces for visible light," Opt. Express **24**, 16309–16319 (2016).